Crystallographic and Optical Spectroscopic Study of Metal–Organic 2D Polymeric Crystals of Silver(I)- and Zinc(II)-Squarates

Bojidarka Ivanova *

Posted Date: 7 October 2024

doi: 10.20944/preprints202410.0388.v1

Keywords: Squarate crystals; zinc(II) and silver(I) coordination compounds; linear and nonlinear optical properties; quantum chemistry

 doi:10.20944/preprints202410.0388.v1

Article

Crystallographic and Optical Spectroscopic Study of Metal–Organic 2D Polymeric Crystals of Silver(I)- and Zinc(II)-Squarates

Bojidarka Ivanova

Lehrstuhl fur Analytische Chemie, Institut fur Umweltforschung, Fakultat fur Chemie und Chemische Biologie, Universitat Dortmund, Otto-Hahn-Strase 6, 44221 Dortmund, Nordrhein-Westfalen, Germany; e-bojidarka.ivanova@yahoo.com or b_ivanova@web.de

Abstract: Metal–organic framework materials show feature linear- and nonlinear optical responses such as laser damage threshold, outstanding mechanical properties, thermal stability, and optical transparency as innovative functional materials for nonlinear optical technologies. The non-centrosymmetric crystal structure is precondition for generation of second-order nonlinear optical response, which guarantees technological applications. The Zn^{II}- and Ag^{I}-squarate complexes are attractive templates for these purposes due to good crystal growth, optical transparency, high thermal stability, etc. However, debatable is the space group type of catena-((μ2-squarato)-tetra-aqua-zinc(II)) complex ($[Zn(C_4O_4)(H_2O)_4]$) (1) showing centro- and non-centro-symmetric monoclinic C2/c and Cc phases. The same is valid to catena-((μ3-squarato)-(μ2-aqua)-silver(I)) complex ($Ag_2C_4O_4$) (2) exhibiting, so far, only C2/c phase. This study reports first new crystallographic data on (1) and (2) re-determined at different temperatures (293(2) and 300(2)K) and non-centro-symmetric Cc phase of (2), having different number molecules per unit cell comparing with C2/c phase. There are high-resolution crystallographic measurements of single crystals, experimental electronic absorption and vibrational spectroscopic data together with ultra-high resolution mass spectrometric ones. Experimental results are supported for theoretical optical and nonlinear optical properties obtained via high accuracy quantum chemical static methods and molecular dynamics, using density functional theory as well as chemometrics.

Keywords: squarate crystals; zinc(II) and silver(I) coordination compounds; linear and nonlinear optical properties; quantum chemistry

1. Introduction

Nonlinear optical crystals have already found indispensable application as optical devices at an industrial scale to laser and telecommunication technologies as sensing or imaging materials, optical switchers, and more. [1–5]. The second harmonic generation is second-order nonlinear optical phenomenon, which is fundamentally important for developing of advanced laser technologies. There is a practical implementation of solid-state lasers having significantly expanded wavelength range, because they generate coherent radiation encompassing from ultraviolet to infrared region; thus, covering a broad spectrum of utilization is for laser medicine, photolithography, military industry, and more. The major process of second harmonic generation is defined as conversion of a certain value of wavelength of light to half of its original value or the order of magnitude of the corresponding frequency is increased two times.

The non-centrosymmetric crystal structure is the precondition for generation of second-order nonlinear optical response of materials, and their high laser damage threshold, which guarantees corresponding practical applications of the nonlinear optical crystals.

On the other hand, the specific case of Pockels effect of crystals has been investigated as well as, due to potential applications of the materials for modulating and switching functions in photonics

 doi:10.20944/preprints202410.0388.v1

[6]. As the second harmonic generation, the Pockels effect is observed also in non-centro-symmetric crystals or centro-symmetric crystals, having strain-induced dielectric susceptibility. The experimental value of the second order dielectric susceptibility of the crystalline sample obtained via second harmonic generation measurements shows the same order of magnitude of as the value related to the Pockels effect.

In the latter context, inorganic nonlinear optical materials frequently provided feature nonlinear optical and linear electro-optic (Pockels effect) response such as laser damage threshold in addition to their outstanding mechanical properties. Due to these reasons, they have been already implemented for decades into generate coherent radiation at wavelengths in technologies where suitable laser sources are not developed, so far.

However, the structural diversity of inorganic NLO materials needs to be extended, due to frequent need of improvement of their liner-optical and NLO performances. The molecular design of inorganic compounds, however, is restricted comparing with organics. Due to the later reasons organic linear-optical and NLO materials provide also prominent molecular crystalline candidates for possess of (non)linear optical technologies, due to their flexible chemical structures and significant capability of chemical substitution. Despite, these advantages of organics, their practical applications have been often restricted, as well as, due to their poor mechanical properties and optical stability in addition to complex synthetic approaches to chemical modification of their molecular structures in order to gain desirable tuned optical, respectively, nonlinear optical properties of the corresponding crystals.

Moreover, in cases of crystals of aromatic organic compounds there can be observed dipole-dipole interactions and antiparallel $\pi \circledcirc \pi$ stacking effects of planar aromatic structures of the molecules; thus, causing for centro-symmetric arrangements of the structural units. In such cases; if any, the electric dipole moments of crystalline molecules is a result from charge transfer. It prevents detection of second harmonic generation performances and Pockels effect.

Fortunately, organic-inorganic hybrid materials show marked structural diversity of MOFs crystals having 0D–3D dimensions and; thus, they can be tailor-made to show high nonlinear optical performances by integrating advantages of inorganic and organic materials. Particularly, their capability of relatively easy reduction of dimensionality comparing with organic crystals could be strengthened; thus, enhancing their stability. The band gap of low-dimensional crystalline structures increases; thus, expanding the wavelength range of second harmonic generation response and improves their laser damage threshold.

Therefore, the question of the symmetry of the molecular crystals, respectively, ionic crystals is central to design and develop liner-optical and nonlinear optical and technologies.

However, frequently crystallographic reports pose a distinctive problem for accurate determining of space-group type of molecular crystals, despite, enormous research effort over decades which has been devoted to implement into the fields of chemical crystallography reliable statistical and chemometric criteria allowing to address reliably the discussed issue (consider detail on [7].)

Despite, available statistical and mathematical methods as well as developed theories detailing on molecular structural analysis via single crystal X-ray diffraction in addition to implemented statistical and mathematical tests dominating in the field of chemical crystallography, due to their powerful capability of distinguishing among subtle variations of crystallographic measurands, the relevant debates in the issue concerning reliability of a determined space group type have begun to flourish [7,8]. The major reasons of the later fact is that (i) the crystallographic structural solution process a set of experimental variables of measurants, where reliability of the structural data depends on uncertainty of measurable parameters; thus, first requiring data-processing of crystallographic data-blocks measured in multiplication in order to assess further the reliability of the final quantitative parameters of the crystallographic structures; (ii) there can be observed spontaneous crystallization of a molecular crystals in two different space-group types [9]; and (iii) frequently there are obtained comparable statistical parameters of structural solutions of a molecular crystalline system into both centro- and non-centrosymmetric space group types [10]. The key aspects of the

 doi:10.20944/preprints202410.0388.v1

discussed issue lie behind aforementioned debates account not only for potential practical applications of crystalline materials, but also for addressing fundamental questions bridging the gap among relations molecular-structure-crystal-structure-molecular properties or in-depth understanding of observable molecular properties and chemical reactivity as well as mechanistic aspects of chemical transformations and reactions in condensed phases, because of single crystal X-ray diffraction as analytical instrumentation plays crucial role in determining experimentally electron density of atoms in molecules; and thus, to determine experimentally not only geometry parameters but also subtle electronic effects; if any.

In addition to non-centrosymmetric crystal structure of materials the second basic prerequisite condition determining molecular, respectively, ionic crystals as suitable NLO-phores is their wide transparency window or absorption edge < 200 nm ($E_g \geq 5.8$ eV). At this point, there should be also mentioned properties such as; for instance, large second harmonic generation coefficient: $d_{ij} > 0.39$ pm.V^{-1} [d_{36}(KDP)] of crystals, their moderate birefringence: $\Delta n \sim 0.07–0.10$ at λ_{ex}=1064 nm; a highlighted chemical stability of materials as well as large laser damage threshold as aforementioned, their easy growth, and high-quality of the single crystalline objects, respectively [2,4].

The challenge of the field of materials research therefore is to obtain crystalline materials with different morphologies and shapes depending on specific purposes of technological application. To solve the problem with non-centrosymmetricity of crystals for purposes of liner-optical and nonlinear optical technologies, first is needed to strictly control molecular, respectively, ionic arrangements in crystals or designing and synthesizing molecular structures, having increased complexity in order to avoid centro-symmetric molecular arrangement in their crystals.

In the latter context and from perspective of the major goal of this study there should be said that squarate-based MOFs evoked a great deal of interest, particularly, highlighting metal squarate $(M^{II}–C_4O_4)_n$ coordination nD polymers [10,11] due to their broad spectrum of technological applications involving catalysis, gas storage technologies; for instance, acetylene or hydrogen storage [12,13], photonics and optoelectronics [14]; luminescent or light emitting diodes [15], materials, having color rendering properties [16], electrochemistry, biomedicine, separation technologies [17], environmental cleaning technologies for treatment of for instance polluted ground and surface water with organics or with metal ions [18], memory devices [19], removal and purification methods, drugs delivery, and more.

Particular, the application of metal-organic frameworks to the field of nonlinear optics has been comprehensively discussed (2024); thus, highlighting their advantages [20,21], because of they represent innovative materials with good crystallinity and mechanical properties [21] as well as a vast variety of symmetry of metal ions/clusters, types of metal chromophores, and type of organic linkers, respectively. The task of crystal engineering, in the later context, dealing with design and synthesis of crystals exhibiting n-dimensional intermolecular, respectively, inter-ionic networks via tuning of hydrogen bond interactions continues to be an important issue, amongst others, in the solid-state crystallographic studies of self-assembly modes or supramolecular chemistry, including of squarete complexes, because of squaric acid (3,4-dihydroxycyclobut-3-ene-1,2-dione) and its mono and dianions are particularly attractive molecular templates for purposes of liner-optical and NLO-materials research and crystal engineering; thus, allowing for modulating the whole range of requested 0D–3D crystalline materials such as, for example complexes $[M^{II}(C_4O_4)(C_4H_4N_2)(H_2O)_4]$ (M = Fe^{II}, Co^{II}, Ni^{II}, Cu^{II}) or $[Mn^{II}_4(C_4O_4)_4(C_4H_4N_2)(H_2O)_8]$ [16,22] showing several supramolecular motifs and metal-to-ligand coordination modes (Figure S1;) thus, yielding to unique structural topologies in its metal-organic coordination polymers. The (hydrogen)squarate ligand(s) readily coordinates and bridge a large number of transition metal ions and ions of lanthanides or actinides; thus, showing variety of structural dimensionalities and coordination modes of mononuclear and binuclear cmplexes [23–25].

Despite, its polycentered coordination capability, anions of squaric acid also coordinate monodentately and bidentate; thus, forming cheating complexes [16,26–28]. Non-centrosymmetric cubic (Pn3n) squarate crystal of {$[ZnC_4O_4.2H_2O).CH_3COOH].H_2O$} has been determined, as well [29]. Crystallographic structural motif of discrete squarate anions has been also determined [30,31]. In

 doi:10.20944/preprints202410.0388.v1

addition, key aspects of coordination capability of squaric acid anions includes forming of 1D polymers and crystals of mixed ligand complexes as well as a capability of stabilizing of doped crystals with tunable mixed metallic doped depending on the requested redox and magnetic properties of the new materials [32–35].

In controlling the structural motifs and symmetry of hybrid squarate-based MOF materials often is difficult to be achieved only via tuning of intermolecular/interionic interactions of species, due to flexible chelation of squarate ligand and process of hydrolysis of many ions of metals. The level of control in the latter processes can be increased through specific chemical substitution of the squarate ligand; thus, introducing specific functional groups allowing to tune stearic effect of ligand and chelation processes of metal ion; thus, directly affecting on dimensionality of crystals and their supramolecular interactions. At this point is should be highlighted that (hydrogen)squarate ligands rapidly, in mild synthetic conditions, and in high yield synthetic yield produce chemical substituted derivatives involving Lewis acid catalyzed condensation reactions; for instance, with anilines or squarate esters, showing a broad spectrum of tunable optical properties [36,37]. The correlation between molecular and crystalline spectroscopic properties are of particular importance in designing of new functional NLO-materials because of both experimental and theoretical spectroscopic tools are used to provide insight into the properties of molecular building units present in designed crystals still at initial synthetic stages of materials research, because of both synthesis of ligands, respectively, coordination compounds as well as crystallization process could lead to difficulties, including those ones associated with correlation between properties of complexes in solution with those one resulted in the solid-state crystalline phase [38]. The latter statement is particularly valid to Zn^{II}- and Ag^{I}-complexes, which often show stable solvate species in solution; thus, dissolving crystalline compounds (see the mass spectrometric data on **(2)**, herein and data on Ag^{I}-complexes with O-containing ligands [39].

Despite, as can be seen in case of $[Zn(H_2O)_6^{2+}]$ counterion containing complexes the coordination species are stable in both crystalline state and solution [40,41]. On this picture, the simplicity of squaric acid anions as ligands, their significant coordination capability toward a broad spectrum of metal ions in addition to diversity of coordination modes and self-assembly (self) associates as well as capability of their rapid chemical substitution in mild synthetic conditions represent crucial advantage of the anions of squaric acid as templates for design of new MOFs with prospective application to the NLO-technologies, among others mentioned, before.

It is, perhaps, time when there should be argued on advantages of Zn^{II}- and Ag^{I}-metal ion containing complexes as MOF NLO-phores. If there are examined particularly optical properties of such compounds, then there should be highlighted their important characteristic qualities such as broad optical transparency window [42] and significant thermal stability, among others [43–49]. Innovations (2024) [21] have shown that Zn^{II}-ion based MOFs with potential application to NLO technologies and tunable NLO responses are characterized by high thermal stability (T=600^{o}C) and third harmonic generation response (3ω) of $2.9.10^{-12}$ esu (λ=1500 nm). However, the presence of 1,1-biphenyl]-4-carboxylic acid and N,N-di(4-pyridyl)-1,4,5,8-naphthalenetetracarboxydiimide ligands cause for relatively restricted transparency window $\lambda_{max} > 600$ nm.

Solid-state TGV data on transition metal ion containing squarates and their mixed ligand derivatives, including the results from the analysis of $[Zn(HC_4O_4)_2(OH_2)_4]$ show high thermal stability of corresponding squarate moieties up to T=400^{o}C [43–49], and depending on type of mixed ligands in inner coordination sphere. The thermal decomposition path of the latter complex is characterized by four stages: $[Zn(HC_4O_4)_2(OH_2)_4] \rightarrow [Zn(HC_4O_4)_2(OH_2)_2]$ (T=161^{o}C) $\rightarrow [Zn(HC_4O_4)_2]$ (T=210^{o}C) $\rightarrow [Zn(HC_4O_4)]$ (T=310^{o}C) $\rightarrow$ [ZnO] (T=400^{o}C) [43].

For purposes of this study its should be underlined that a vast amount of work has been performed in determining molecular and crystal structure of (1) because of it is obtained not only in rapid interaction and excellent crystal growth of high quality single crystals (see [49],) but also both the squarates and hydrogen squarates frequently show pressure induced change of their lattice structure from monoclinic-to-tetragonal one, respectively, change of their asymmetric-to-centrosymmetric crystalline structures, particularly highlighting hydrogen squarate compounds [50].

 doi:10.20944/preprints202410.0388.v1

There should be mentioned that crystal structure of hydrogen squarate complex $[Zn(HC_4O_4)(H_2O)_4]$ is a centrosymmetric triclinic one having space group type P-1 (Table 1 [43]).

However, debatable is space group type of Zn(II)-ion containing squarate crystal catena-((μ-squarato)-tetra-aqua-zinc(II)) ($[Zn(C_4O_4)(H_2O)_4]$) studied in this work, as well. Research effort so far has shown that it crystallized both centro- and noncentrosymmetrically monoclinic space group types C2/c [51,52] and Cc [9].

Since, the crystallographic refinement conditions only show *h k l* with $h + k = 2n$ and *h0l* with $l = 2n$ or space groups Cc or C2/c, then the final solution and description of the crystal structure of the discussed complex has to be made in non-centrosymmetric group type Cc [9]. There is found a support for this view looking at the obtained low R_1-parameter of structural solution showing R_1=0.023 (see Table 1 and data on work [9].)

Therefore, we have not seen objective reason to reject the latter view looking closer at available experimental facts. As an effort to obtain non-centrosymmetric phase of the complex this study re-determined the crystal structure of catena-((μ$_2$-squarato)-tetra-aqua-zinc(II)) (1) in triplication at different temperatures T=293(2) and 300(2)K; thus, obtaining, however a centrosymmetric phase, having C2/c space group type (see Table 1, CCDC 1917571, 1917547, and 1565990). The new results support the view of work [51] determining crystallographically the same analyte at T=120(2)K. To the question, however, "Does the solution of the crystal structure should be in monoclinic noncentrosymmetric space group type Cc?" this work provides an answer to it solving the structure of the complex CCDC 1917547 ((1)_2) into Cc space group type. There is obtained non only an increasing in R_1-parameter from R_1=0.058 (C2/c) to 0.0782 (Cc) in addition to results from symmetry tests suggesting the former space group type (see, below.)

The results from work [51] and new data on complex (1) do not reject, however, the view that the discussed compound could crystallize into non-centrosymmetric space group type Cc. Due to further results in this study, it is possible to admit that in certain experimental crystallization conditions complex (1) should produce noncentrosymmetric crystals. The latter position could be hold looking at new crystallographic results reported first, herein, of catena-((μ$_3$-hydrogen squarato)-(μ$_2$-aqua)-silver(I)) (2) (CCDC 2387639 and 2387641). As crystal structure of complex (1) the Ag(I)-coordination compound crystallizes in monoclinic space group type C2/c (CCDC 771415, [53,54]) measured at T=199(2) K. The new data on the same complex at T=300(2) K (CCDC 2387641, Table 2) agree with previously reported data.

Table 1. Crystallographic refinement data on catena-((μ-hydrogen squarato)-tetra-aqua-zinc(II)) and catena-((μ$_2$-squarato)-tetra-aqua-zinc(II)); (1)_1 and (1)_2 denote data of a single crystal of complex catena-((μ$_2$-squarato)-tetra-aqua-zinc(II)) measured in duplication at different temperatures, while (1)_3 denotes data on the complex measured from different single crystal of the sample.

Complex	$[Zn(HC_4O_4)(H_2O)_4]$	$[Zn(C_4O_4)(H_2O)_4]$	
CCDC	929462	-	-
Ref.	[43]	[51]	[9]
Empirical formula	$C_8H_{10}O_{12}Zn$	ZnC4O4,4H2O	ZnC4O4,4H2O
Moiety formula	$C_8H_{10}O_{12}Zn$	'C8 O16 Zn2'	'C8 O16 Zn2'
Formula mass	-	249.48	-
Crystal system	Triclinic	Monoclinic	Monoclinic
Space Group	P-1	C2/c	Cc
a [Å]	5.0919(5)	8.986(2)	9.012(2)
b [Å]	7.3113(7)	13.333(2)	13.336(3)
c [Å]	8.7536(7)	6.694(3)	6.746(2)
α [°]	66.440(6)	90.00	90.00

 doi:10.20944/preprints202410.0388.v1

β [°]	77.254(7)	99.67(2)	99.33(2)
γ [°]	75.480(7)	90.00	90.00
V [Å^3]	286.50(5)	790.6(3)	800.0
Z	1	4	-
p[g.cm^{-1}]	2.107	2.096	2.07
F000	184	-	-
μ(Mo-K) [mm^{-1}]	2.216	31.9	-
T [K]	100 (2)	120(2)	-
θ range	4.68– 29.66	40–90	-
Refl. collected	3003	19653	2639
Unique refl.	1308	4140	-
R1[2σ(I)]	0.0513	0.023	-
*R*1 (all data)	0.0534	0.024	0.039
wR2	0.1325	0.024	0.042
GooF	1.092	-	-
Diff. peak/ hole [e/Å^3]	1.464/ -1.792	0.79/-1.13	-
Complex	[Zn(C_4O_4)(H_2O)$_4$]		
CCDC	1917571	1917547	1565990
Single crystal	(1)_1	(1)_2	(1)_3
Ref.	This work [55]	This work [56]	This work
Empirical formula	ZnC4O4,4H2O	ZnC4O4,4H2O	ZnC4O4,4H2O
Moiety formula	'C8 O16 Zn2'	'C8 O16 Zn2'	C4 O8 Zn
Formula mass	482.82	482.82	241.41
Crystal system	Monoclinic	Monoclinic	Monoclinic
Space Group	C2/c	C2/c	C2/c
a [Å]	9.003(3)	9.003(3)	8.982(3)
b [Å]	13.295(5)	13.295(5)	13.315(5)
c [Å]	6.746(3)	6.746(3)	6.734(3)
α [°]	90.00	90.00	90.00
β [°]	99.244(17)	99.244(17)	99.327(15)
γ [°]	90.00	90.00	90.00
V [Å^3]	797.0(5)	797.0(5)	794.7(5)
Z	2	2	4
p[g.cm^{-1}]	2.012	2.012	2.018
F000	472	472	472
μ(Mo-K) [mm^{-1}]	3.095	3.095	3.104
T [K]	293(2)	300(2)	293(2)
θ range	4.33–25.29	4.33–25.11	2.76–25.12
Refl. collected	1180	1157	1200
Unique refl.	643	641	586

 doi:10.20944/preprints202410.0388.v1

R1[2σ(I)]	0.0796	0.0581	0.0608
*R*1 (all data)	0.0906	0.1562	0.0660
wR2	0.1937	0.1532	0.0721
GooF	1.013	1.383	1.128
Diff. peak/ hole [e/Å^3]	1.414/-1.477	0.674/-1.059	1.835/-1.344

Table 2. Crystallographic refinement data on catena-((μ$_3$-squarato)-(μ$_2$-aqua)-silver(I)).

Complex	$[Ag(C_4O_4)O]_n$	$[Ag(C_4O_4)O]_n$	$[Ag(C_4O_4)O]_n$
CCDC	771415	2387639	2387641
Single crystal	(2)_1	(2)_2	(2)_3
Refs.	[53,54]	This work	This work
Empirical formula	C_4AgO_5	C_4AgO_5	C_4AgO_5
Moiety formula	C_4AgO_5	C_4AgO_5	C_4AgO_5
Formula mass	235.91	459.81	235.91
Crystal system	Monoclinic	Monoclinic	Monoclinic
Space Group	C2/c	Cc	C2/c
a [Å]	13.572(9)	13.491(11)	13.594(6)
b [Å]	8.229(6)	8.233(11)	8.251(3)
c [Å]	11.108(7)	11.038(13)	11.107(4)
α [°]	90.00	90.00	90.00
β [°]	118.142(17)	117.94(5)	118.094(11)
γ [°]	90.00	90.00	90.00
V [Å^3]	1093.9(12)	1083(2)	1099.0(7)
Z	8	4	8
p[g.cm^{-1}]	2.865	2.820	2.852
F000	888	864	888
μ(Mo-K) [mm^{-1}]	3.561	3.666	3.617
T [K]	199(2)	300(2)	300(2)
θ range	3.00–25.07	3.01–24.94	3.00–25.24
Refl. collected	3173	1555	1655
Unique refl.	951	1034	963
R1[2σ(I)]	0.0558	0.1544	0.2323
*R*1 (all data)	0.0587	0.1781	0.0944
wR2	0.1819	0.3626	0.1044
GooF	0.952	2.026	1.003
Diff. peak/ hole [e/Å^3]	2.591/ -1.161	3.374/-2.879	3.344/-1.724

However, as the later tabulated parameters reveal there is obtained a non-centrosymmetric monoclinic phase of complex (2) showing Cc space group type. The application of symmetry tests [7] (see below) shows a lack of additional symmetry operations. In addition, the crystallographic solution in centrosummetric space group type C2/c shows increasing in R_1-parameter up to R_1=0.1746. The same is valid to a structural solution in I2/c space group type. The latter new results together

 doi:10.20944/preprints202410.0388.v1

with those ones reported previously clearly show that, despite the research effort, so far, knowledge of crystallization behavior of even simple squatates and hydrogen squarate crystals of Zn(II)- and Ag(I)-ions do not imply knowledge of what is preferred monoclinic space group type looking at C2/c and Cc ones, and depending on experimental conditions of synthesis and crystal growth. The similarity of crystallization preference of the two Zn(II) and Ag(I)-ions and common space group types of their coordination species with squaric acid anions assume that there is a practical relation between coordination capability of the ions and the squarate ligands. The current study in the later context contributes crucially to further understanding of the issue which is closely related not only to the fundamental issue of chemical crystallography associated with development of robust tests for unambiguous determining of space group types of crystals [7], but also to practical fields of NLO-phore research of MOFs based new materials, due to a set of advantages which possess squarate crystals of Zn(II)- and Ag(I)-ions.

Further arguments and results shedding light on the latter issue should be even particularly valid and important because of Ag(I) and Zn(II)-complexes often crystallize into monoclinic C-type space groups showing possible or pseudo new space group type Cc which refinements are often unstable [53]. In other words, complexes of Zn(II) and An(I)-provide a prospective templates for design of new MOFs NLO-phores, due to their tend to produce non centro-symmetrical crystals.

Owing to the fact that the purpose of this study is twofold, the paper provide theoretical and experimental linear optical and NLO-properties of crystals (1) and (2) in condensed phases using crystallographic data on both the centro- and non centrosymmetric space group types. The stability of complexes (1) and (2) in solution detailed on perspective of experimental optical spectroscopic and ultrahigh resolution mass spectrometric results from electrospray ionization measurements. The latter arguments are particularly important regarding common statements that optical, respectively, NLO-properties of crystals could be related to those ones in solution, which are true ones only when the coordination compounds are stable in the two phases, i.e., solution and crystalline state ones.

As section “Abstract” has already summarized the paper also provides experimental and theoretical data on single crystal X-ray diffraction, Fourier transform infrared spectroscopic and high accuracy static and molecular dynamics results from molecular and crystalline structures, optical and NLO- properties of coordination species (1) and (2).

Since, the molecular design, synthesis, crystallographic analysis, and spectroscopic studies—both the theoretical and experimental ones — are the primary focuses on MOF materials research as well as it is a strategic step in constructing new and specific supramolecular arrangements of crystals, then an in-depth comprehension of correlation among molecular structure, crystal structure, and physical–optical–chemical properties of new functional materials contribute crucially to develop the filed of MOFs based materials research.

2. Materials and Methods

2.1. Synthesis

The complexes (1) and (2) were obtained by mixing of $ZnCl_2.2H_2O$ (0.1773 g) or $AgNO_3$ (0.1690 g) inorganic salts with 25 mL squaric acid (0.115 g, Sigma) in solvent mixture methanol:water 1:2 under stirring for 1 h at T=200°C. Yields 70% (1) and 38% (2). Analytical calculations for complex $[Zn(C_4O_4).4H_2O]$ (1): C, 19.26; H, 3.23; O, 51.30. Found (1): C, 19.28; H, 3.20%. Analytical calculations for complex $[C_4O_5Ag]$ (2): C, 20.37; O, 33.91. Found (2): C, 20.33%. The single crystals of the analytes were obtained using slow evaporation approach to ambient conditions for 10 days. Consider detail on [53].

2.2. Analytical Instrumentation

The X-ray diffraction hkl-intensities were obtained using Bruker Smart X2S diffractometer, and micro source Mo Ka radiation; thus, employing the ω scan mode. The crystal structures of complexes (1) and (2) in Figure 1 are presented using PLATON [57]. The absorption correction method utilized for the purposes of the crystallographic solution was based on multiple scanned reflections. The

 doi:10.20944/preprints202410.0388.v1

crystal structures were solved by direct methods using SHELXS-97 and were refined by full matrix least-squares refinement against F^2 [58–60]. Anisotropic displacement parameters were introduced for all non-hydrogen atoms. The experimental refinement parameters are summarized in Tables 1 and 2.

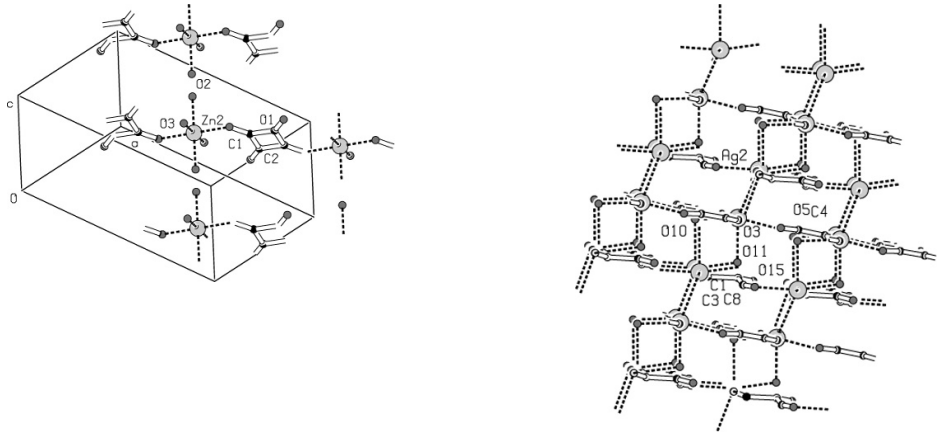

(1) (CCDC 1565990); single crystal (1)_3 (2) (CCDC 2387639); single crystal (2)_2

Figure 1. PLUTON plots of crystal structures of complexes (1) and (2).

The monopole and multi-pole electron density refinement was carried out by means of XD2016 and MoPro v16 program packages [61–65]; thus, employing the Hansen–Coppens methodology. The experimental structural factors were further processed by WinGX 2014 [66] towards data quality. WTANAL and DRK plot analyses of the structure factors were carried out. In addition, to residual analyses and THMA were performed; thus, evaluating the thermal motion on the basis of the experimentally measured U_{ij} values [67,68].

HPLC–ESI-tandem MS/MS measurements were performed on TSQ 7000 instrument (Thermo Fisher Inc., Rockville, MD, USA), using mobile phase compositions 0.1% (*v*/v) aqueous solution of HCOOH, 0.1% (v/v) HCOOH in CH_3CN; 20.0% (v/v) HCOOH in CH_3CN:CH_3OH solvent mixture 1:1; and 10.0% KOH/$NaCO_3$ in CH_3OH. A triple quadruple mass spectrometer (TSQ 7000 Thermo Electron, Dreieich, Germany) equipped with an ESI 2 source was employed for ESI-MS measurements under experimental conditions: Capillary temperature 275.00°C; sheath gas 50.00 psi, source voltage 5 kV and cappylary voltage 33.95 V; cappilary temperature -63.17°C. Samples of complexes were dissolved in CH_3CN (1 mg.mL^{-1}) and were injected in the ion source by an auto sampler (Surveyor) with a flow of pure CH_3CN (0.2 mL.min^{-1}). The data were processed by Excalibur 1.4 software. An overall mass range was m/z 100–600. A standard LTQ Orbitrap XL (Thermo Fisher Inc.) instrument was employed, as well. The chromatographic analysis was performed with a Gynkotek (Germering, Germany) HPLC instrument, equipped with a preparative Kromasil 100 C18 column (250x20 mm, 7 μm; Eka Chemicals, Bohus, Sweden) and a UV-detector set at 250 nm. The mobile phase is CH_3CN:H_2O (90:10, v/v) at a flow rate of 4 mL.min^{-1}. The analytical HPLC was performed on a Phenomenex (Torrance, CA, USA) RP-18 column (Jupiter 300 150x2 mm, 3 μm) under the shown conditions. The analysis was carried out using Shimadzu UFLC XR (Kyoto, Japan) instrument, equipped with an auto-sampler, PDA, an on-line degasser and column thermostat. As stationary phase a Phenomenex Luna Phenyl-Hexyl column (150x3mm i.d., 3 μm particle size) was used. The mobile phase consisted of 0.02% (v/v) TFA in water (solvent A) and CH_3CN:CH_3OH 75:25 (v/v; solvent B). Separation was achieved by a gradient analysis starting with 55A–45B, increasing the amount of B in 30min to 75 % and 30.1 min to 100 % B, stop time 40 min.

The IR-spectra were measured on a Bomem Michelson 100 FTIR spectrometer (4000–400 cm^{-1}, ±1 cm^{-1} resolution, and 200 scans. It is equipped with a Specac wire-grid polarizer. The data were processed via GRAMS AI 7 software (Thermo Fisher Scientific Inc.)

The UV–VIS–NIR spectra were recorded on Evolution 300 spectrometer within the 190–1100 nm range.

 doi:10.20944/preprints202410.0388.v1

2.3. Theory/Computations

The GAUSSIAN 98, 09; Dalton2011 and Gamess-US [69–71] program packages were used. The output files were visualized by GausView03 [72]. Ab initio and DFT molecular optimization was carried out by means of B3LYP, B3PW91 and ωB97X-D methods, respectively. The Truhlar's functional M06-2X was used, as well [73,74]. The algorithm by Bernys was taken into determine the ground state. The stationary points at the potential energy surface (PES) were obtained by harmonic vibrational analysis. The criterion confirming minima of the energy is the absence of imaginary frequencies (negative eigenvalues) of second-derivative matrix. The basis set cc-pVDZ by Dunning, 6–31+ + G(2d,2p), quasirelativistic effective core pseudo potentials from Stuttgart-Dresden(-Bonn) (SDD,SDDAll, https://www.cup.uni-muenc hen.de/oc/zipse /losalamos-natio nal-labor atory -lanl-ecps.html), and LANL2DZ were used [75]. The zero point vibrational energy and vibrational contributions have been accounted for up to a magnitude value of 0.3 eV. Species in solution were examined by of explicit super molecule and "mixed" approach of micro hydration. The polarizable continuum method is used. The effect of the ionic strengths in solution was accounted for integral-equation-formalism polarizable continuum model. Merz-Kollman atomic radii and heavy atoms UFF topological models were used. Large species were treated using own N-layer integrated molecular orbital and molecular mechanics method. The electrostatic potentials and natural bond orbital (NBO) methods are applied, as well. The molecular dynamics was performed by ab initio or DFT Born Oppenheimer approach. It was also carried out at M062X functional and SDD or cc-pvDZ basis sets, without to consider periodic boundary condition. The trajectories were integrated using Hessian-based predictor–corrector approach with Hessian updating for each step on Born—Oppenheimer potential energy surface. The stepsizes were 0.3 and 0.25 amu/Bohr. The trajectory analysis stops when: *(a)* centres of mass of a dissociating fragment are different at 15 Bohr, or *(b)* when the number of steps exceed the given to as input parameter maximal number of points. The total energy was conserved during the computations within at least 0.1 kcalmol-1. The analysis was performed by fixed trajectory time speed (t = 0.025 or fs) starting from initial velocities. The velocity Verlet and Bulirsch-Stoer integration approaches were used. The Allinger's molecular mechanics force field MM2 was also employed [76]. The low order torsion terms is accounted with higher priority rather than van der Waals interactions. The accuracy of the method comparing with experiment is 1.5 kJ.mol-1 studying diamante [77]. The differences in heats of formation of alcohols and ethers is |0.04|–|6.02| kJ.mol-1.

Crystallographic structural data on complexes (1) and (2) were used to input atomic coordinates during quantum chemical computations.

Calculations of electron absorption spectra were performed using exchange correlation potential and including scalar-relativistic effects. The electronic absorption spectra were obtained by electronic excitation computations within linear response in time dependent density functional theory and the Tamm–Dancoff approximation [78–80], showing exellent predictive capability of electronic spectra of MOFs [19].

2.4. Chemometrics

The software R4Cal Open Office STATISTICs for Windows 7 was used. The statistical significance was checked by *t*-test. The model fit was determined upon by F-test. Analysis of variance was also used [81–86]. Together with ANOVA test, there are used nonparameteric two sample Kolmogorov–Smirnov [87], Wilcoxon–Mann–Whitney [88], and Mood's mediantests [89], as well.

3. Results

3.1. Chromatographic and Mass Spectrometric Data on Solution

As there is already told [39–41], the proper experimental and theoretical design of MOF-based material research is actually in successful operation only when there is reliable assignment of the coordination species in both the solution and in the solid crystalline state. Chromatographic and mass spectrometric data on complex (2) show that at RT=14.34 mins there are observed MS peaks at m/z

 doi:10.20944/preprints202410.0388.v1

145/147 of Ag^{I}-hydride complex of type $[Ag^{I}H(H_3O^{+})(H_2O)]$. As can be seen the oxidation state of the metal ion is kept (+1).

Conversely, Zn^{II}-complexes of simple O-containing organic ligands often produce solvate complexes of the zinc metal ions in different oxidation states (consider detail on [40,41].)

3.2. Crystallographic Data

The crystal structure of complex $[Zn(C_4O_4)(H_2O)_4]$ (1) at T=120 K [51] reported previously and herein (CCDC 1917571 [55], 1917547 [56], and 1565990 (this work), Table 1 and Figure 1) at T=293(2) and 300(2) K are the same. Furthermore, the four complex species are isostructural and crystallize in monoclinic and centrosymmetric space group type C2/c. There is a lack of discrepancy between the reported three independent structural solutions of the three new crystals (1)_1, (1)_2, and (1)_3 and results from applying ADDSYM test used to PLATON software [57], which is capable of reliable distinguishing between centro- and non-centrosymmetric space-group types [7]. A pro-argument for the latter statement is reached testing the structural solution of crystallographic data-block of the structure of the same complex CCDC 1917547 solved into non-centrosymmetric monoclinic space group type Cc (supporting information). As Figure S3 reveals, the ADDSYM test shows missing or additional symmetry operations and suggests solution in C2/c space group type. Despite, the fact that the structural solution in Cc space group type shows low R_1-parameter (R_1=0.0782, supporting information,) the determination of the crystal structure is performed using the ADDSYM criterion; thus, yielding to R_1=0.0581 (Table 1) in C2/c space group type.

The Zn(II)-ion in complex (1) exhibits distorted octahedral geometry of the metal chromophore $Zn^{II}O_6$ showing r(Zn–O) bond lengths of 2.068, 2.072, and 2.129 Å (Figure 1.) The corresponding bond angles ∠(O–Zn–O) vary as followings: 88.08, 88.54, 88.68, 91.46, and 94.42°, respectively. The squarate dianion shows $\mu_{1,3}$-bonding type and acts as bridging ligand. The interplanar angle between squarate p-aromatic systems is 5.02°, while the interplane distance is 3.559 Å (Figure 2.)

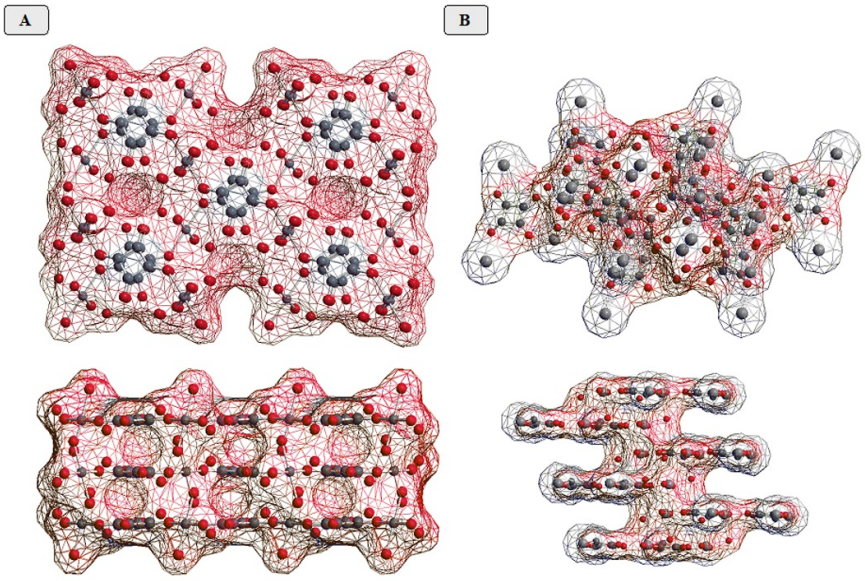

Figure 2. Crystallographic packing of molecules of the unit cell of the crystals (1) (A) and (2) (B) viewed from different perspectives; solvent accessible surfaces.

The comparative analysis with the crystal structure of the corresponding hydrogen squarate complex $[Zn(HC_4O_4)_2(OH_2)_4]$ [43] shows that again the metal ion is coordinated in a distorted octahedral geometry of the $Zn^{II}O_6$ metal chromophore connected with four O-centres of the solvent water molecules and two monodentately bonded hydrogen squarate anions HC4O4- arranged

 doi:10.20944/preprints202410.0388.v1

mutually in a trans-configuration. The molecular chains of the crystal are interconnected by $[Zn(OH_2)_4]^{2+}$ structural sub-units.

Works [53,54] briefly touched on the coordination capability of Ag(I) with squarate dianion showing that the complex catena-((μ_3-squarato)-(μ_2-aqua)-silver(I)) (2) (CCDC 771415, T=199(2)K) form a stable square pyramidal geometry of the Ag^IO_5 metal chromophore, thus exhibiting bond lengths r(Ag–O) = 2.317, 2.352, 2.498, and 2.512 Å of the equatorial Ag–O bonds as well as 2.613 Å of the axial Ag–O bond. Consider data on crystal (2)_1 in Table 2. This study, reports re-determination of the crystal structure of the same complex obtained due to independent synthesis (crystal (2)_3, CCDC 2387641) at different temperature T=300(2) showing again good crystal growth and low R_1 parameter (R_1=0.0944) despite the fact that it is determined at higher temperature. The crystallographic refinement data show good agreement with the results from works [53,54] showing again centrosymmetric space group type C2/c. Owing to the fact that the ADDSYM test used to PLATON software [57] confirms the same space group type there could be claimed that the structural analysis is free of mistake.

However, the purpose of the current study is not to provide only new crystallographic data of the same complex at different temperature of crystallographic measurements, but merely to discuss the affect of the independent measurements in multiplication of one and the same coordination compounds on the crystallographic parameters because of routinely as aforementioned such data are used to predict theoretically linear-optical and nonlinear optical properties of the crystals among other ones. Thus, the variation of experimental geometry parameters affects on the energetics of the molecular crystals. Since, the theoretical quantum chemical data involve high accuracy determining of the energy parameter among other molecular properties up to six decimal sign as can be expected the variation of the initial atomic coordinates of the molecules in the computed crystals should affect on the theoretical parameters, as well. The later issue seemed of significant importance due to the fact that subtle electronic effects could be accounted for with significant error only as a result for variation of crystallographic inputs of the theoretical computations. The study tackles the latter topics following the route in its explaining in the chemometrics. As ANOVA data on **Table S1** show the two datasheets of crystallographic variables of crystals (2)_1 and (2)_3 are statistically not significantly different. Therefore, they belong to the same complex (2) having C2/c space group type. Within the framework of multiplication of measurements, thus, the geometry parameters should be tackled with the corresponding standard deviations; thus, yielding to a=13.58375±0.01534, b=8.24045±0.01534, c=11.10805±9.19239.10^{-4} Å; β=118.11814±0.03398^o, V=1096.491±3.64726 Å^3 and r=2.8585±0.00919 g.cm^{-1}. As can be seen within the framework of multiple crystallographic re-determinations the accuracy of the input atomic coordinates affect on the second decimal sign, and thus properties of such crystals could be reliably predicted with relatively low cost computational approaches. As can be expected, depending on the number of theoretical computations both the energy parameters should account of the uncertainty of the input crystallographic atomic coordinates.

In addition to new crystallographic data on complex (2) obtained ad different experimental conditions, the current study reports new non centrosymmetry phase of the complex (2) crystallizing into monoclinic space group type Cc (CCDC 2387639, crystal (2)_2.) The application of ADDSYM test used to PLATON software shows in this case a lack of missing or additional symmetry operation (Figure S4.)

At this point, if one is asked to criticize anything in what there is written, perhaps there should be only two objections worth mentioning, which this study shall briefly address. The first objection is that the current paper claims for new non-centrosymmetry crystalline phase of the same complex (2), but not for new non-centrosymmetric complex of Ag(I) ion with squarate anionic ligand. The major reason for the latter statement is that the geometry parameters of crystals (2)_1 or (2)_3 of the centrosymmetric phases are statistically none significantly different from the experimental parameters of the non-centrosymmetric phase (2)_2 (Table S2). Therefore, despite the fact that there are reported different crystallographic structural data from independent crystals obtained in independent synthetic experimental conditions, the experimentally determined unit cell parameters

 doi:10.20944/preprints202410.0388.v1

are statistically not distinguishable mutually, and thus the corresponding data belong to different crystallographic symmetry phases of the same complex (2), but not to different complexes.

In order to satisfy the readers straightaway on all possible objections, next there is addressed a second objection related with structural solution of crystal (2)_2 in centrosymmetric space group system C2/c. The corresponding CIF data on the latter solution are shown in the supporting information file, as well. As can be seen, it shows higher R_1-parameter (R_1=0.1746) comparing with the solution of the complex in a non-centro-symmetry phase Cc. The same is valid to solve the discussed structure into I2/c space group type. Thus, in order to arrive at an empirically evident knowledge of the true space group type of crystalline phase (2)_2 of complex (2) (CCDC 2387639) there are used two arguments, i.e., (i) from the ADDSYM test of symmetry; and (ii) the R1-parameter, which convinced me; thus, I am able to convince the reader that the latter phase is non centrosymmetric one, rather than a centrosymmetric phase. As an attempt to grasp completely the discussed issue there should be highlighted that the structural solution of (2)_2 in Cc space group type was not performed on the base on the statement above that when there are two solutions of a crystalline phase there should be carried out the non-centrosymmetric one [9]. Rather, as the statistical data show the statistical and chemometric performances of the crystallographic solution into Cc space group type are better than those one of the centrosymmetric solution. Therefore, the final structural solution of (2)_2 was based on objective criteria on statistical and chemomeric tests.

The crystal structure consists of square pyramidal $Ag^{I}O_5$ metal chromophore showing bond lengths *r*(Ag–O) = 2.545, 2.522, 2.333, and 2.410 Å of the equatorial Ag–O bonds as well as 2.426 Å of the axial Ag–O bond. The ∠(O–Ag–O) bond angles are 88.3(5), 89.9(8), 87.7(6), and 94.8(8)o, respectively. By contrast to centrosymmetric phase (2)_1 containing Z=8, the crystal structure of the non-centrosymmetric phase Cc is characterized by Z=4 or there are four complex molecules in the unit cell. The two O-centers act as bridging ligands between two Ag^{I}-ions, showing *r*(Ag–O) = 2.426 and 2.668 Å. The corresponding bond angles ∠(Ag–O–Ag) are 91.4(0) and 98.2(3)^{o}. There is distance *r*(Ag···Ag)=3.587 Å. The complex is characterized by high thermal stability up to 480 K. The thermoanalytical data on Ag^{I}-complex of squarate dianions detailing on the decomposition reactions has been performed [90,91]. There has been proposed the following decomposition reaction $Ag_2C_4O_{4(s)} + CO_{(g)} \rightarrow 2Ag_{(s)} + CO_2 + [C_4O_3]$ at T=515–535 K [90]. Despite, the fact that as aforementioned the Ag^{I}-complexes show significant stability of their (+1) oxidation state of the metal center, there has been proposed stable Ag^{2+} species at T = 485–500 K, as well [91]. There has been proposed the following reaction: $Ag_2C_2O_4 \rightarrow Ag^0 + \{Ag^{2+}(C_4O_4)^{2-}\}$.

3.3. Electronic Optical Properties in Solution

Looking at electronic absorption properties of the two complexes (1) and (2) in solution they shall be described as virtually closed to each other, due to determine by the mass spectrometric data stable solvate complexes of the metal ions (see sub-Section 3.1.) The observed experimentally electronic absorption bands within the UV-range of the electromagnetic spectrum (Figure 3), therefore, should be assigned to electronic transition within the framework of the squarate anions or the ligands. The experimental data are explained well enough via theoretical quantum chemical computations. As can be seen the employment in SOS/DQ or EOM approaches and LANL2DZ basis set to crystallographic data on the complex species or to their optimized geometries (below) yields to difference between the experimental and theoretical λ_{max} of the electronic absorption spectra of 3.65 nm (see also Figure S5 and Table S3.) The observed UV-bands as can be expected are assigned to n→p transitions of squarate dianion. The obtained theoretical value λ_{max}=268.77 nm (*f*=0.3538) agree excellent with the experimental data in CH_3OH or H_2O reported to this study as well as data on other authors showing that the squarate dianion exhibits two characteristic absorption maxima at 272 (4.55 eV) and 252 nm (4.90 eV) [92].

 doi:10.20944/preprints202410.0388.v1

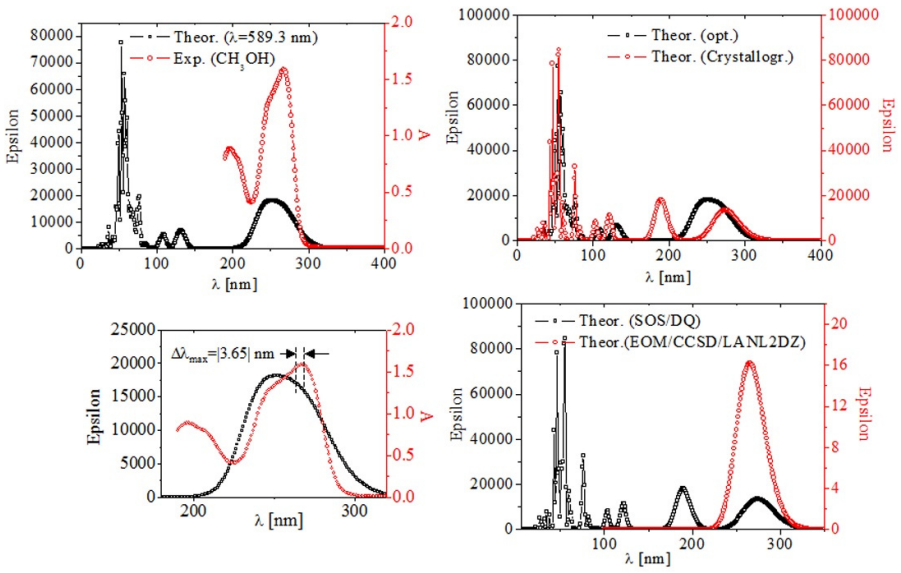

Figure 3. Experimental and theoretical (M062X/LANL2DZ) spectra of crystal of (2) and its optimized molecular geometry at various level of theory; the experimental spectra were measured in solvent water.

Apart from the highlighted above advantages of the complex (2) as prospective new MOF based NLO-phore such as its non-centrosymmetric crystalline phase and high temperature stability up to T=535 K, there should be added the optical transparence of the crystals within 270–1100 nm.

3.4. Vibrational Properties in Crystalline State

The vibrational modes of the crystalline materials are studied both theoretically and experimentally, herein. The theoretical analysis is based on the optimized geometry of the two Zn^{II}- and Ag^{I}-complexes of squarate ligand. Table S4 summarizes the energetics of the optimized species, using the atomic coordinates as shown in Table S5. The obtained vibration modes in ground states are tabulated, as well (Table S6.) Figure S6 in the later context illustrates theoretical IR spectra together with selected visualized vibrational motions of the species. The IR-bands at 1804–1750, 1620, and 1530 cm^{-1} belong to $\nu_{C=O}$, $\nu_{C=C}$, and $\nu_{C=C}+\nu_{C=O}$ stretching vibrations of squarate ligand. The bands within 1460–1100 cm^{-1} are assigned to ν_{C-C} stretching mode, while the band at 727 cm^{-1} belong to ring breathing vibration. The IR bands at 650 and 317 cm^{-1} correspond to δ_{ring} and δ_{CO} modes. The shown experimental and theoretical data on M062X/LANL2DZ agree well with results from comprehensive analysis of vibrational properties of squarate complex species of alkali metal ions [93], as well. To ν_{Zn-O} stretching vibration of Zn^{II}-squarate complex there has been assigned Raman mode at 385 cm^{-1} (λ_{ex}=514.5 nm) [94].

3.5. Nonlinear Optical Properties

In this sub-section the author would like to add that the claim regarding prospective application of complex (2) to linear-optical and nonlinear optical technologies is based not only the fact that it is among the rare cases of Ag^{I}-complexes of squarates which crystallizes non centrosymmetrically — there are at about 15 % of the reported crystals of Ag^{I}-ion and at about 13 % of complexes of Zn^{II}- and Ag^{I}-ions with the discussed ligand crystallized into non centrosymmetric space group type (**Table S7**) — or it shows significant thermal stability and optical transparency within 200–1100 nm, but also looking at theoretical linear optical and nonlinear optical properties. The comparative analysis involves data on the complex (2) and the squarate dianion. There are obtained the following results from polarizability and hyper polarizability tensor components [$(C_4O_4)^{2-}$] (polar. 85.1708865, -

 doi:10.20944/preprints202410.0388.v1

0.000005, 85.1471524, -0.0001605, 0.0005283, 23.2082861; hyper polar. -0.0098898, 0.1864671, -0.0071, 0.275977, 0.0786893, -0.1005592, 0.0792977, -0.0001254, 0.0049768, 0.0518928); (2) (polar. 259.6438627, -5.2250367, 168.1356433, 1.5268616, -0.1398028, 62.4900084; hyper polar. -8.6881902, -27.0819917, 6.9304239, -0.4725642, -4.9880504, 3.8684769, 1.0596874, -0.8279703, -2.8137591, -3.4648956.) As can be seen there is increasing in α_{xx} tensor component of magnitude order 3.04 times, and 879.43 times the β_{xxx} tensor component in the complex comparing with the free squarate dianionic ligand. Those readers who give the mater attention concentrating on the latter data and results from KDP—inorganic material with marked NLO properties which is already used to the field of the nonlinear optical technologies as highlighted above—shall clearly see that the α_{xx} value of complex (2) have larger value of magnitude order of 7.00 times comparing with KDP computed at the same level of theory (KDP (polar. 37.0776932, -0.000518, 32.6220945, -0.0037454, -3.1567931, 32.8203542; hyper polar. -234.6417743, 0.0909451, -38.4587409, -0.1151177, -0.0412643, -41.1818089, 0.0247814, -53.9553874, -0.026954, -0.0198434.)

Table 3 summarizes the frequency dependent dipole polarizability and first dipole hyper polarizability. The data on KDP are listed in Table S8. As can be seen $\beta(-\omega,\omega;0)_{||(z)}$ (ω=455.6 nm) of (2) is 3.64 times large than the value of KDP, while $\beta_{zzz}(-\omega,\omega;0)$ of the complex is 2.255 times large comparing with the KDP one.

The results from the latter tables are in accordance with what the author is taught, i.e., that the metal-organic framework materials based on Ag^{I}-or Zn^{II}-complexes of squarate ligands produce comparable linear optical and nonlinear optical responses to marked inorganic NLO materials such as the used standard KDP one.

Table 3. Electric dipole moment [(Debye = 10^{-18} statcoulomb cm, SI units = Cm), dipole polarizability, α (esu units = cm^3, SI units = $C^2m^2J^{-1}$), and first dipole hyperpolarizability, β, where || and _|_ denote parallel and perpendicular components, (z) with respect to z axis, as well as vector components x, y, and z (esu units = $statvolt^{-1}.cm^4$, SI units = $C^3.m^3.J^{-2}$) data on complex (2).

Electric dipole moment			
	[a.u.]	Debye	10^{-30} SI
μ_{tot}	0.317187D-01	0.806208D-01	0.268922
μ_x	0.000000	0.000000	0.000000
μ_y	0.000000	0.000000	0.000000
μ_z	0.317187D-01	0.806208D-01	*0.268922*
Dipole polarizability			
$\alpha(0,0)$	[au]	[10^{-24} esu]	[10^{-40} SI]
α_{iso}	0.425867D+03	0.631070D+02	0.702160D+02
α_{aniso}	0.986272D+03	0.146150D+03	0.162614D+03
α_{xx}	0.633700D+03	0.939047D+02	0.104483D+03
α_{yx}	0.103717D+03	0.153692D+02	0.171006D+02
α_{yy}	0.154964D+03	0.229634D+02	0.255502D+02
α_{zx}	-0.500754D+03	-0.742041D+02	-0.825632D+02
α_{zy}	-0.495223D+02	-0.733845D+01	-0.816513D+01
α_{zz}	0.488936D+03	0.724529D+02	0.806147D+02
$\alpha(-\omega,\omega)$ ω=455.6 nm	[au]	10^{-24} esu	10^{-40} SI
α_{iso}	0.153553D+03	0.227542D+02	0.253175D+02
α_{aniso}	0.587493D+03	0.870575D+02	0.968645D+02
α_{xx}	0.327207D+03	0.484871D+02	0.539492D+02

 doi:10.20944/preprints202410.0388.v1

α_{yx}	0.227125D+02	0.336565D+01	0.374479D+01
α_{yy}	-0.970495D+02	-0.143813D+02	-0.160013D+02
α_{zx}	-0.241757D+03	-0.358247D+02	-0.398603D+02
α_{zy}	-0.815340D+02	-0.120821D+02	-0.134431D+02
α_{zz}	0.230502D+03	0.341568D+02	0.380046D+02
First dipole hyperpolarizability			
β(0;0,0)	[a.u.]	[10^{-30} esu]	[10^{-50} SI]
$\beta_{\|\|(z)}$	0.450178D+01	0.388919D-01	0.144343D-01
$\beta_{\_\|\_(z)}$	0.150059D+01	0.129640D-01	0.481145D-02
β_x	-0.369368D+02	-0.319105	-0.118433
β_y	-0.124310D+02	-0.107394	-0.398583D-01
β_z	0.225089D+02	0.194459	0.721717D-01
$\beta_{\|\|}$	0.900112D+01	0.777627D-01	0.288609D-01
β_{xxx}	-0.819435D+01	-0.707928D-01	-0.262740D-01
β_{xxy}	-0.923337D+01	-0.797692D-01	-0.296055D-01
β_{yxy}	-0.164386D+01	-0.142017D-01	-0.527081D-02
β_{yyy}	-0.358041D+01	-0.309320D-01	-0.114801D-01
β_{xxz}	0.736136	0.635964D-02	0.236032D-02
β_{yxz}	-0.210114D+01	-0.181522D-01	-0.673702D-02
β_{yyz}	-0.191303D+01	-0.165271D-01	-0.613386D-02
β_{zxz}	-0.247405D+01	-0.213738D-01	-0.793269D-02
β_{zyz}	0.867012D+01	0.749031D-01	0.277995D-01
β_{zzz}	0.867986D+01	0.749873D-01	0.278308D-01
β(-ω,ω,0) ω= 455.6 nm			
	[a.u.]	[10^{-30} esu]	[10^{-50} SI]
$\beta_{\|\|(z)}$	-0.106836D+04	-0.922982D+01	-0.342556D+01
$\beta_{\_\|\_(z)}$	-0.999635D+02	-0.863607	-0.320519
β_x	0.408269D+04	0.352712D+02	0.130906D+02
β_y	-0.271454D+04	-0.234515D+02	-0.870381D+01
β_z	-0.534181D+04	-0.461491D+02	-0.171278D+02
$\beta_{\|\|}$	0.145013D+04	0.125280D+02	0.464965D+01
β_{xxx}	0.396853D+03	0.342850D+01	0.127246D+01
β_{yxx}	0.621301D+02	0.536756	0.199212
β_{yyx}	-0.322483D+03	-0.278600D+01	-0.103400D+01
β_{zxx}	-0.327435D+03	-0.282878D+01	-0.104987D+01
β_{zyx}	-0.113067D+03	-0.976813	-0.362535
β_{zzx}	0.279499D+03	0.241465D+01	0.896175
β_{xxy}	-0.425822D+03	-0.367877D+01	-0.136534D+01
β_{yxy}	0.705009D+03	0.609073D+01	0.226051D+01
β_{yyy}	-0.423235D+03	-0.365642D+01	-0.135704D+01

 doi:10.20944/preprints202410.0388.v1

β_{zxy}	0.496533D+03	0.428966D+01	0.159207D+01
β_{zyy}	-0.962529D+03	-0.831550D+01	-0.308622D+01
β_{zzy}	-0.752474D+03	-0.650079D+01	-0.241270D+01
β_{xxz}	-0.843863D+03	-0.729032D+01	-0.270573D+01
β_{yxz}	0.220077D+03	0.190130D+01	0.705647
β_{yyz}	0.322371D+03	0.278504D+01	0.103364D+01
β_{zxz}	0.762547D+03	0.658781D+01	0.244500D+01
β_{zyz}	-0.195401D+03	-0.168811D+01	-0.626526D+00
β_{zzz}	-0.746798D+03	-0.645175D+01	-0.239450D+01

4. Conclusions

So a reasonable conclusion from this study might be that it deals with new, firstly reported in the literature non centro-symmetric phase of catena-((μ_3-squarato)-(μ_2-aqua)-silver(I)) complex of Ag^I-ion and squarate ligand crystallizing into monoclinic Cc space group type. It shows high thermal stability up to T=535 K, good crystal growth, an optical transparency within 264–1100 nm; and thus, it appears a prominent candidate for metal-organic framework based linear optical and nonlinear optical crystalline material. In addition, the complex shows both in solution and in the solid state high stability of AgI-oxidation state of the metal center. This conclusion is drawn on the base on a long-standing opinion that the non centro-symmetric crystal structure is the precondition—in addition to outstanding mechanical properties of the crystals—for generation of second-order nonlinear optical response of crystalline materials, and their high laser damage threshold, which guarantees practical applications of the designed crystals to nonlinear optical technologies. Perhaps, there may be one who would prefer to highlight the novelty of the study also reporting data on crystallographic re-determination in multiplication of catena-((μ2-squarato)-tetra-aqua-zinc(II)) at different experimental conditions toward temperature; thus, discussing the affect of uncertainty of crystallographic variables on theoretically predicted optical and nonlinear optical properties of the materials together with their energetics, which the current study also has provided. Furthermore, the study has tackled from perspective of statistical tests data on multiplication measurements of complex catena-((μ_3-squarato)-(μ_2-aqua)-silver(I)), as well as, in addition to detail correlation between molecular structure crystal structure and optical properties both the experimentally and theoretically. However, the author has arrived at the present conclusion in order to underline prospective application of the studied complexes as innovative metal-organic framework based materials to many interdisciplinary branches of technology and industry, rather, than to focus the reader attention on their affect on the fundamental science connected with further in-depth understanding of the coordination chemistry of transition metal ions with d^{10}-electronic configuration or the chemical crystallography, among others.

Supplementary Materials: The following supporting information can be downloaded at the website of this paper posted on Preprints.org, Mass spectrometric, chromatographic, and infrared spectrometric both experimental and theoretical data as well as chemometrics (Figures S1–S6 and Tables S1–S8). CCDC 1565990, 2387639, 2387641 contain the supplementary crystallographic data on ZnII- and AgI-complexes with squarate ligand. The data can be obtained free of charge via http://www.ccdc.cam.ac.uk/conts/retrieving.html, or from the Cambridge Crystallographic Data Centre, 12 Union Road, Cambridge CB2 1EZ, UK; fax: (+44) 1223-336-033; or e-mail: deposit@ccdc.cam.ac.uk.

Author Contributions: Conceptualization, B.I.; methodology, B.I.; software, B.I.; validation, B.I.; formal analysis, B.I.; investigation, B.I.; resources, B.I.; data curation, B.I.; writing—original draft preparation, B.I.; writing—review and editing, B.I.; visualization, B.I.; supervision, B.I.; project administration, B.I.; funding acquisition, B.I.

Funding: This research was funded by Deutsche Forschungsgemeinschaft (Funder ID: http://dx. doi.org/10.13039/50110 00016 59); grant 255/22–1.

 doi:10.20944/preprints202410.0388.v1

Acknowledgments: The author is grateful to thank the Alexander von Humboldt Foundation for the Fellowships and the donation of single crystal X-ray diffractometer to the Department of Analytical Chemistry at the Faculty of Chemistry and Pharmacy at the Sofia University St. Kl. Ohridsk; the Deutsche Forschungsgemeinschaft (Funder ID: http://dx. doi.org/10.13039/50110 00016 59; for the grant 255/22–1 of metal-organics materials research;) the Deutscher Akademischer Austausch Dienst for grant within priority program Stability Pact South-Eastern Europe, and the central instrumental laboratory clusters for mass spectrometry (currently, Centre of Mass Spectrometry) at Dortmund University..

Conflicts of Interest: The author declares no conflict of interest.

References

1. Qi, S., Cheng, P., Han, X., Ge, F., Shi, R., Xu, L., Li, G., Xu, J. Organic-inorganic hybrid antimony(III) halides for second harmonic generation. *Cryst. Growth Des*. **2022**, *22*, 6545–6553.
2. Halasyamani, P., Zhang, W. Viewpoint: Inorganic materials for UV and deep-UV nonlinear-optical applications. *Inorg. Chem*. **2017**, *56*, 12077–12085.
3. Liang, H., Yang, Y., Shao, L., Zhu, W., Liu, X., Hua, B., Huang, F. Nanoencapsulation-induced second harmonic generation in pillararene-based host-guest complex cocrystals. *J. Am. Chem. Soc*. **2023**, *145*, 2870–2876.
4. Liu, M., Tang, X., Zhang, Y., Ren, J., Wang, S., Wu, S., Mi, J., Huang, Y. Strategy for a rational design of deep-ultraviolet nonlinear optical materials from zeolites. *Inorg. Chem*. **2023**, *62*, 15527–15536.
5. Meena, M., Ebinezer, B., Manikandan, E., Sundararajan, R., Shalini, M., Natarajan, R. Synthesis and optical characterizations of L-phenylalanine lithium sulphate (LPLS) semi-organic single crystal. *J Mater Sci: Mater Electron* **2023**, *34*, 395.
6. Manganelli, C., Pintus, P., Bonati, C. Modeling of strain-induced Pockels effect in silicon. *Opt. Expr.* **2015**, *23*, 28649.
7. Ivanova, B. Comment on "Comment on "Crystallographic and theoretical study of the atypical distorted octahedral geometry of the metal chromophore of zinc(II) bis((1R,2R)-1,2-diaminocyclohexane) dinitrate"". *J. Mol. Struct*. **2023**, *1287*, 135746.
8. Ivanova, B., Spiteller, M. Noncentrosymmetric organic crystals of barbiturates as potential nonlinear optical phores: experimental and theoretical analyses. *Chem. Pap*. **2019**, *73*, 2821–2844.
9. Weiss, A., Riegler, E., lt, I., Böhme, H., Robl, C. Transition metal squarates, I. Chain structures $M(C_4O_4).4H_2O$. *Z. Naturforsch.* **1986**, *41b*. 18–24.
10. West, R. Niu, H. New aromatic anions. VII. Complexes of saquarate ion with some divalent and trivalent metals. *J. Am. Chem. Soc.* 1963, 85, 2589–2590.
11. Jayaramulu, K., Krishna, K., George, S., Eswaramoorthy, M., Maji, T. Shape assisted fabrication of fluorescent cages of
12. squarate based metal–organic coordination frameworks. *Chem. Commun.* **2013**, ***49***, 3937–3939.
13. Li, H., Wang, J., Zhai, Q. Development of MOF-5-like ultra-microporous metal-squarate frameworks for efficient acetylene storage and separation. *J. Mater. Chem*. A **2023**, *11*. 21203–21210.
14. Yilmaz, H., Andac, O., Gorduk, S. Synthesis, characterization, and hydrogen storage capacities of polymeric squaric acid complexes containing 1-vinylimidazole. *Polyhedron* **2017**, *133*, 16–23.
15. Xu, X., Zhou, J., Shi, Z., Kuai, Y., Hu, Z., Cao, Z., Li, S. Microwave-assisted in-situ synthesis of low-dimensional perovskites within metal-organic frameworks for optoelectronic applications. *Appl. Mater. Today* **2024,** *40*, 102418.
16. Seco, J., Calahorro, A., Sebastian, E., Salinas-Castillo, A., Colacio, E., Rodriguez-Dieguez, A. Experimental and theoretical study of photoluminescence and magnetic properties of metal–organic polymers based on squarate and tetrazolate moieties containing linkers. *New J. Chem*. **2015**, *39*, 9926–9930.
17. Stone, J., Decoteau, E., Polinski, M. Synthesis and structural characterization of an air and water stable divalent Europium squarate prepared by in situ reduction. *J. Solid State Chem*. **2021**, *297*, 122048.
18. Mani, C. Berthold, T., Fechler, N. Cubism on the nanoscale: From squaric acid to porous carbon tubes. *Small* **2016**, *21*, 2906–2912.
19. Vatani, P., Aliannezhadi, M., Tehrani, F. Improvement of optical and structural properties of ZIF-8 by producing multifunctional Zn/Co bimetallic ZIFs for wastewater treatment from copper ions and dye. *Sci. Rep*. **2024**, *14*, 15434.
20. Getzner, L., Paliwoda, D., Vendier, L., Lawson-Daku, L., Rotaru, A., Molnar, G., Cobo, S., Bousseksou, A. Combining electron transfer, spin crossover, and redox properties in metal-organic frameworks. *Nat. Commun.* **2024**, *15*, 7192.
21. Kenzhebayeva, Y., Kulachenkov, N., Rzhevskiy, S., Slepukhin, P., Shilovskikh, V., Efimova, V., Alekseevskiy, P., Gor, G., Emelianova, A., Shipilovskikh, S., Yushina, I., Krylov, A., Pavlov, D., Fedin, V., Potapov, A., Milichko, V. Light-driven anisotropy of 2D metal-organic framework single crystal for repeatable optical modulation. *Commun. Mater***. 2024**, *5*, 48.

 doi:10.20944/preprints202410.0388.v1

22. Yuan, H., Xu, X.; Qiao, X.; Kottilil, D., Shi, D., Fan, W.; Yuan, Y.; Yu, X.; Babusenan, A.; Zhang, M.; Ji, W. Tunable nonlinear optical properties based on metal-organic framework single crystals. *Adv. Optical Mater*. **2024**, *12*, 2302405.
23. Wang, C.; Chung, W.; Lin, H.; Dai, S.; Shiu, J.; Lee, G.; Sheu, H.; Lee, W. Assembly of two Zinc(II)-squarate coordination polymers with noncovalent and covalent bonds derived from flexible ligands, 1,2-*bis*(4-pyridyl)ethane (dpe). *CrystEngComm* **2011**, *13*, 2130–2136.
24. Li, J.; Yin, M.; Li, Y.; Wang, C. Uncommon 3D twofold interpenetrated zinc phosphate consisting of inorganic chains and mixed ligands for highly efficient dye removal ability using its nanosized particles. *Inorg. Chem*. **2022**, *61*, 7964–7969.
25. Wang, C.; Ke, S.; Hsieh, Y.; Huang, S.; Wang, T.; Lee, G.; Chuang, Y. Water de/adsorption associated with single-crystal-to-single crystal structural transformation of a series of two-dimensional metal-organic frameworks, [M(bipy)(C_4O_4)(H_2O)$_2$].3H_2O (M = Mn, Fe, and Zn, and bipy = 4,4′-bipyridine). *J. Chin. Chem. Soc*. **2019**, *66*, 1031–1040.
26. Mautner, F.; Fischer, R.; Grant, A.; Romain, D.; Salem, N.; Louka, F.; Massoud, S. Copper(II) and zinc(II) complexes bridged by benzenoid aromatic oxocarbon and dicarboxylate dianions. *Polyhedron* **2023**, *234*, 116327.
27. Dan, M.; Sivashankar, K.; Cheetham, A.; Rao, C. Amine-templated metal squarates. *J. Solid State Chem*. **2003**, *174*, 60–68.
28. Basile, M.; Unruh, D.; Streicher, L.; Forbes, T. Spectral analysis of the uranyl squarate and croconate system: Evaluating differences between the solution and solid-state phases. *Cryst. Growth Des*. **2017**, *17*, 5330–5341.
29. Weiss, A.; Riegler, E.; Robl, C. Ubergangs metallquadratate, III Über die trikline Käfigstruktur des (MC_4O_4.2H_2O).3 CH_3COOH.H_2O (M = Zn^{2+}, Mn^{2+}). *Z. Naturforsch.* **1986**, *41b*, 1333–1336.
30. Weiss, A.; Riegler, E.; Robl, C. Transition metal squarates, On the Structure of cubic (MC_4O_4.2H_2O).CH_3COOH.H_2O (M = Zn^{2+}, Ni^{2+}). *Z. Naturforsch.* **1986**, *41b*, 1329–1332.
31. Kirchmaier, R.; Altin, E.; Lentz, A. Crystal structure of tetraaqua-2-pyrazine-zinc(II) squarate, [Zn(H_2O)$_4$($C_4H_4N_2$)](C_4O_4). *Z. Kristallogr*. NCS **2004**, *219*, 33–34.
32. Ucar, I.; Karabulut, B.; Bulut, A.; Bueyue kguengoer, O. Synthesis, crystal structure, Cu^{2+} doped EPR and voltammetric studies of *bis*[N-(2-hydroxyethyl)ethylenediamine]zinc(II) squarate monohydrate. *J. Phys. Chem. Solids* **2007**, *68*, 45–52.
33. Bulut, A.; Ucar, L.; Kalyoncu, T.; Yerli, Y.; Bueyuekguengoer, O. Structural and magnetic properties of one-dimensional squarate bridged coordination polymers containing 2-aminomethylpyridine ligand. *J. Inorg. Organomet. Polym*. **2010**, *20*, 793–801.
34. Wang, C.; Yang, C.; Lee, G.; Tsai, H. Syntheses, structures, and magnetic properties of two 1D, mixed-ligand, metal coordination polymers, [M(C_4O_4)(dpa)(OH_2)] (M = Co^{II}, Ni^{II}, and Zn^{II}; dpa = 2,2′-dipyridylamine) and [Cu(C_4O_4)(dpa)(H_2O)]$_2$.(H_2O). *Eur. J. Inorg. Chem*. **2005**, *2005*, 1334–1342.
35. Razavi, S.; Chen, W.; Zhou, H.; Morsali, A. Tuning redox activity in metal–organic frameworks: From structure to application. *Coord. Chem. Rev*. **2024**, *517*, 216004.
36. Yang, C.; Chuo, C.; Lee, G.; Wang, C. Self-assembly of two mixed-ligands metal-organic coordination polymers. Inorganic *Chem. Commun*. **2003**, *6*, 135–140.
37. Rostami, A.; Colin, A.; Li, X.; Chudzinski, M.; Lough, A.; Taylor, M. N,N′-diarylsquaramides: General, high-yielding synthesis and applications in colorimetric anion sensing. *J. Org. Chem.* **2010**, *75*, 3983–3992.
38. Piggot, P.; Seenarine, S.; Hall, L. Complexes of aminosquarate ligands with first-row transition metals and lanthanides: New insights into their hydrolysis. *Inorg. Chem*. **2007**, *46*, 5243–5251.
39. Xu, X.; Zhou, J.; Shi, Z.; Kuai, Y.; Hu, Z.; Cao, Z.; Li, S. Microwave-assisted in-situ synthesis of low-dimensional perovskites within metal-organic frameworks for optoelectronic applications. *Appl. Mater. Today* **2024**, *40*, 102418
40. Ivanova, B.; Spiteller, M.; Stochastic dynamic electrospray ionization mass spectrometric diffusion parameters and 3D structural determination of complexes of Ag^{I}-ion—experimental and theoretical 3 treatment. *Int. J. Mol. Liq*. **2019**, *292*, 111307.
41. Ivanova, I.; Spiteller, M. Electrospray ionization mass spectrometric solvate cluster and multiply charged ions ⊚ a stochastic dynamic approach to 3D structural analysis. *SN Appl. Sci.* **2020**, *2*, 731.
42. Ivanova, I.; Spiteller, M. Electrospray ionization stochastic dynamic mass spectrometric 3D structural analysis of Zn^{II}-ion containing complexes in solution. *Inorg. Nano-Met. Chem*. **2022**, *52*, 1407–1429.
43. Khan, S.; Mir, M. Photomechanical properties in metal-organic crystals. *Chem. Commun.* **2024**, *60*, 7555–7565.
44. Serb, M.; Braun, B.; Oprea, O.; Dumitru, F. Synthesis, crystal structure and thermal decomposition study of new [tetraaqua-bis-(monohydrogensquarate)]zinc(II) complex. *Digest J. Nanomater. Biostruct*. **2013**, *8*, 797–804.
45. Mondal, A.; Das, D.; Chaudhuri, N. Thermal studies of nickel(II) squarate complexes of triamines in the solid state. *J. Therm. Anal. Cal*. **1999,** *55*, 165–173.

46. Maji, T.; Das, D.; Chaudhuri, N. Preparation, characterization and solid state thermal studies of cadmium(II) squarate complexes ofhane-1,2-diamine and its serivatives. *J. Therm. Anal. Cal*. **2001**, *63*, 617–627.
47. Das, D.; Ghosh, A.; Chaudhuri, N. Preparation, characterization, and solid state thermal studies of nickel(II) squarate complexes of 1,2-Ethanediamine and its derivatives. *Bull. Chem. Soc. Jpn*. **1997**, *70*, 789–797.
48. Maji, T.; Das, D.; Chaudhuri, N. Thermal studies of copper(II) squarate complexes of diamines in the solid state. *J. Therm. Anal. Cal*. **2002**, *68*, 319–328.
49. Yeşilel, O.; Ölmez, H.; Soylu, S. Synthesis and spectrothermal studies of thermochromic diamine complexes of cobalt(III), nickel(II) and copper(II) squarate. Crystal structure of $[Co(en)_3](sq)_{1.5}.6H_2O$. *Trans. Met. Chem.* **2006,** *31*, 396–404.
50. Schaeffer, H. Squaric acid: Reactions with certain metals. *Michrochem. J.* **1972**, *17*, 443–455.
51. Moritomo, Y.; Koshihara, S.; Tokura, Y. Asymmetric-to-ceritrosymmetric structure change of molecules in squaric acid crystal: Evidence for pressure-induced change of correlated proton potentlats. *J. Chem. Phys*. **1990**, *93*, 5429–5435.
52. Lee, C.; Wang, C.; Chen, K.; Lee, G.; Wang, Y. Bond characterization of metal squarate complexes $[M^{II}(C_4O_4)(H_2O)_4$; M = Fe, Co, Ni, Zn, *J. Phys. Chem. A* **1999**, *103*, 156–165
53. Robl, C.; Kuhs, W. Hydrogen bonding in the chain-like coordination polymer $ZnC_4O_4.4H_2O$: A neutron diffraction study. *J. Solid State Chem*. **1988**, *75*, 15–20.
54. Ivanova, B.; Spiteller, M. Ag^{I} and Zn^{II} complexes with possible application as NLO materials—crystal structures and properties. *Polyhedron* **2011**, *30*, 241–245.
55. Ivanova, B.; Spiteller, M. CCDC 771415: Experimental crystal structure determination, **2011** [DOI: 10.5517/cctwqcr].
56. Ivanova, B.; Spiteller, M. CCDC 1917571: Experimental crystal structure determination, **2019** [DOI: 10.5517/ccdc.csd.cc22cd40].
57. Ivanova, B.; Spiteller, M. CCDC 1917547: Experimental crystal structure determination, **2019**, [DOI: 10.5517/ccdc.csd.cc22ccc6].
58. Spek, A. Single-crystal structure validation with the program PLATON. *J. Appl. Cryst*. **2003**, *36*, 7–13.
59. Sheldrick, G.M. A short history of SHELX. *Acta Crystallogr. A* **2008**, *64*, 112–122.
60. Sheldrick, G.M. Experimental phasing with SHELXC/D/E: combining chain tracing with density modification. *Acta Crysallogr.* D **2010**, *66*, 479–485.
61. Sheldrick, G.M. Phase annealing in SHELX-90: direct methods for larger structures. *Acta Crystallogr. A* **1990,** *46*, 467–473.
62. Blessing, R. An empirical correction for absorption anisotropy. *Acta Crystallogr*. **1995**, *A51*, 33–38.
63. Spek, A. Single-crystal structure validation with the program PLATON. *J. App.Crystallogr.* 2003, 36, 7–13.
64. [http://www.ccp14.ac.uk/ccp/web-mirrors/mallinson/~paul/xd.html (XD2016)]
65. Momma, K.; Ikeda, T.; Belik, A.; Izumi, F. Dysnomia, a computer program for maximum-entropy method (MEM) analysis and its performance in the MEM-based pattern fitting. *Powder Diffr*. **2013**, *28*, 184–192.
66. [http://www.crystallography.fr/crm2/fr/services/logiciels/MoPro.htm]
67. [http://www.chem.gla.ac.uk/~louis/software/wingx/]
68. Dunitz, J.; Schomaker, V.; Trueblood, K. Interpretation of atomic displacement parameters from diffraction studies of crystals. *J. Phys. Chem.* **1988**, *92*, 856–867.
69. Dunitz, J.; Maverick, E.; Trueblood, K. Atomic Motions in Molecular Crystals from Diffraction Measurements. *Angew. Chem. Int Ed*. **1988**, *27*, 880–895.
70. Frisch, M.; Trucks, G.; Schlegel,. H et al. (2009) (1998), Gaussian 09, 98. Gaussian Inc, Pittsburgh
71. [https ://www.dalto nprogram.org/download.html]
72. Gordon, M.; Schmidt, M. Advances in electronic structure theory: GAMESS a decade later. In: Dykstra C, Frenking G, Kim K, Scuseria G (eds) Theory and Applications of Computational Chemistry: the first forty years. Elsevier, Amsterdam, 2005, pp 1167–1189
73. [www.gauss ian.com/g_prod/gv5.htm]
74. Zhao, Z.; Truhlar, D. Density functionals with broad applicability in chemistry. *Acct.s Chem. Res*. **2008,** *41*, 157–167.
75. Zhao, Y.; Truhlar, D. The M06 suite of density functionals for main group thermochemistry, thermochemical kinetics, noncovalent interactions, excited states, and transition elements: two new functionals and systematic testing of four M06-class functionals and 12 other functionals. *Theor. Chem. Acct*. **2008**, *120*, 215–241.
76. Hay, P.; Wadt, W. Ab initio effective core potentials for molecular calculations. Potentials for K to Au including the outermost core orbitals. *J. Chem. Phys*. **1985**, *82*, 299.
77. Burkert, U.; Allinger, N. Molecular mechanics in ACS Monograph 177. American Chemical Society, Washington DC, 1982, pp 1–339
78. Allinger, L. Conformational analysis. 130. MM2. A hydrocarbon force field utilizing V1 and V2 torsional terms. *J. Am. Chem. Soc.* **1977,** *99*, 8127–8134.

79. Casida, M. Time-dependent density functional response theory for molecules. In Recent Advances in Density Functional Methods 155–192 (World Scientific, 1995).
80. Van Gisbergen, S.; Snijders, J.; Baerends, E. Implementation of time-dependent density functional response equations. *Comput. Phys. Comm*. **1999**, *118*, 119–138.
81. Hirata, S.; Head-Gordon, M. Time-dependent density functional theory within the Tamm–Dancoff approximation. *Chem. Phys. Lett*. **1999**, *314*, 291–299.
82. Kelley. C. Iterative Methods for optimization, SIAM Front. Appl. Mathematics, 2009; 18.
83. Otto. M. Chemometrics, 3rd ed. Wiley, Weinheim, 2017; pp. 1-383.
84. [http://de.openoffice.org].
85. Madsen, K.; Nielsen, H.; Tingleff, T. Informatics and mathematical modelling, 2nd Ed. DTU Press, 2004.
86. Miller, J.; Miller. J. Statistics and chemometrics for analytical chemistry. Pentice Hall, London, 1988; pp. 1–271.
87. Taylor, J. Quality assurance of chemical measurements. Lewis Publishers, Inc. Michigan, 1987, pp. 1–328.
88. Schroee, G.; Trenkler, D. Exact and randomization distributions of Kolmogorov–Smirnov tests two or three samples. *Comput. Stat. Data Anal*. **1995**, *20*, 185–202.
89. Fay, F.; Proschan, M. Wilcoxon–Mann–Whitney or t-test? On assumptions for hypothesis tests and multiple interpretations of decision rules. *Stat. Surv*. **2010**, *4*, 1–39.
90. Freidlin, B.; Gastwir. J. Should the median test be retired from general use? *Am. Stat.* **2000**, *54*, 161–164.
91. Brown, M.; Kelley, H.; Galwey, A.; Mohamed, M. A thermoanalytical study of thermal decomposition of silver squarate. *Thermochim. Acta*.**1988**, *127*, 139–158.
92. Galwey, A.; Mohamedt, M. Brown, M. Thermal decomposition of silver squarate. *J. Chem. Soc.Faraday Trans. 1* **1988**, *84*, 57–64.
93. Schwartz, L.; Howard, L. Electronic structure of aqueous squaric acid and its anions. *J. Phys. Chem*. **1973**, *77*, 314–318.
94. Georgopoulos, S.; Diniz, R.; Yoshida, M.; Speziali, N.; dos Santos, H.; Junqueira, G.; de Oliveira, L. Vibrational spectroscopy and aromaticity investigation of squarate salts: A theoretical and experimental approach. *J. Mol. Struct*. **2006**, *794*, 63–70.
95. Santos, P.; Amaral, J.; de Olivieira, L. Raman spectra of some transition metal squarate and croconate complexes. *J. Mol. Struct.* **1991**, *243*, 223–232.